Inter-laminar shear stress in hybrid CFRP/austenitic steel

J. Lopes, M. Freitas
ICEMS and Departamento de Engenharia Mecânica. Instituto Superior Técnico. Universidade de Lisboa. Av. Rovisco Pais 1049-001 Lisboa. Portugal
joao.ribeiro.lopes@ist.utl.pt

D. Stefaniak
DLR, Institute of Composite Structures and Adaptive Systems, Ottenbecker Damm 12, 21684 Stade, Germany

P.P. Camanho
IDMEC. Pólo FEUP. Rua Dr. Roberto Frias. 4200-465 Porto. Portugal

ABSTRACT. Bolted joints are the most common solution for joining composite components in aerospace structures. Critical structures such as wing to fuselage joints, or flight control surface fittings use bolted joining techniques. Recent research concluded that higher bearing strengths in composite bolted joints can be achieved by a CFRP/ Titanium hybrid lay-up in the vicinity of the bolted joint. The high costs of titanium motivate a similar research with the more cost competitive austenitic steel. An experimental program was performed in order to compare the apparent inter-laminar shear stress (ILSS) of a CFRP reference beam with the ILSS of hybrid CFRP/Steel beams utilizing different surface treatments in the metallic ply. The apparent ILSS was determined by short beam test, a three-point bending test. Finite element models using cohesive elements in the CFRP/Steel interface were built to simulate the short beam test in the reference beam and in the highest inter-laminar shear stress hybrid beam. The main parameters for a FEM simulation of inter laminar shear are the cohesive elements damage model and appropriate value for the critical energy release rate. The results show that hybrid CFRP/Steel have a maximum ILSS very similar to the ILSS of the reference beam. Hybrid CFRP/Steel is a competitive solution when compared with the reference beam ILSS. FEM models were able to predict the maximum ILSS in each type of beam.

KEYWORDS. Fracture; Fatigue; Durability; Case studies; Experimental techniques; Numerical techniques.

INTRODUCTION

Composite materials have been used in aerospace applications in the past four decades. Their use has grown in the share of weight of aircrafts (from the very specific use in nose cones and radomes of the Airbus A300 to the full barrel composite fuselage of the Boeing 787) and also in complexity. The development of composite manufacturing has enabled the shift from rather simple shells and sandwich structures to full composite assemblies like elevators, horizontal and vertical tail planes, and the already mentioned full barrel composite fuselage. This shift from modular architecture to integral architecture [1] has had many advantages: It has reduced the number of components of an assembly and therefore the number of fasteners. It has simplified the manufacturing process by reducing the number

of parts to manufacture and to assemble. A composite component, however complex, still needs to be assembled to other components.
Bolted joints are the most common joining technique between composite components. Bolted joints offer the advantage of being capable of carrying large loads, are simple to install and to inspect.
This type of joint is more challenging in composite structures than in metallic structures due to their low bearing strength, high notch sensitivity, brittle and anisotropic nature, and high dependence on composite configuration.
The typical solution to joint composite parts is to do a thickness build-up in the vicinity of the bolted area. This solution leads to an increase in weight, therefore cost, and additional stresses caused by eccentricities.
The research work of the German Aerospace Centre with other partners has demonstrated that a significant improvement in bearing load can be achieved by replacing some CFRP plies by metallic plies in the vicinity of the bolted area.
Fink and Kolesnikov [2] demonstrated the suitability of hybrid CFRP/Metal composites in experimental tests using CFRP and Ti6Al4V alloy. The inter-laminar shear stress was measured using the short beam test method in several conditions of temperature and humidity. Bearing ultimate strength tests were also performed with different ratios of Ti alloy contents. It was concluded that hybrid CFRP/Ti has a high bearing strength, high shear strength, and high compression strength. Also, the hybrid specimens have a low sensitivity to temperature and humidity.
Kolesnikov and Fink [3] performed impact tests, bearing tests and dynamic tests in CFRP/Ti6AL-4V. The research concluded that compressive strength of hybrid material is higher than monolithic CFRP; the bearing tests using a three row bolted joint showed that CFRP/TI has a joint efficiency over 65% in the case of a 0º-on axis loading, and a satisfactory fatigue behaviour.
Camanho et al. [4] investigated the experimental and numerical response of bolted joints using a hybrid CFRP and Ti–15V–3Cr–3Sn–3Al alloy with several percentages of Ti content. The experimental results showed that the bearing strength increases with the increase of Ti content, a hybrid joint with 50% titanium has a higher specific stiffness than the reference monolithic CFRP; the critical region in a hybrid joint is the bolt-bearing region and not the transition zone from hybrid to CFRP; The numerical models yielded good results in predicting the bearing strength of hybrid and monolithic composites.
Fink et al. [5] investigated the mechanical response and the manufacturability of hybrid CFRP/Ti alloy in a spacecraft payload adaptor. Using CFRP and Ti–15V–3Cr–3Sn–3Al the research concluded that the CFRP/metal hybridization had, among others, the advantages of high bearing, shear and pull-out strength, high specific bearing strength, and considerable weight savings.
Fink and Camanho [6] performed inter-laminar shear stress by the use of the short beam method and experimental and numerical response of the bearing strength of a hybrid CFRP/Ti alloy. This research concluded that hybrid bearing strength increase to a factor of 2.5 when compared with typical CFRP laminates. Also it concluded for the feasibility and mechanical effectiveness of hybrid joints.
All the previous works were done using titanium alloys as reinforcement material. However the use of steel was already considered as a potential alternative to titanium [5, 6]. Titanium has the advantage of high specific strength, galvanic compatibility, and lower coefficient of thermal expansion (CTE) than corrosion resisting steel. Corrosion resisting steel has the advantage of higher stiffness, higher ultimate strength, excellent fatigue properties and much lower cost when compared with Ti alloys. It has the disadvantage of having a higher CTE producing a significant residual thermal stress. Although these stresses are not addressed in the present work, Stefaniak et. al could show that due to mechanical interaction, residual stresses in multi-layered FMLs are lower than often assumed when only thermo-mechanical behavior is considered [7]. Additionally, by modifications in the curing process, the "smart curing" [8], residual stresses can be lowered significantly.
In this research the objective is to measure the inter-laminar shear stress in a hybrid CFRP/Steel composite.
This research comprises an experimental test program and a numerical simulation in a finite element commercial package. The test program is exposed in detail as well as the numerical simulations. The results of both the experiments and the simulations are presented and compared.

EXPERIMENTAL TESTING

An experimental program on apparent inter-laminar shear stress (ILSS) was determined by short beam three-point bending tests with two main objectives: i) to identify the most suitable surface treatment method for the metal foil in this particular fibre metal laminate; ii) to determine the required cohesive element parameters to simulate delamination failure.

Stainless steel 1.4310 (X10CrNi18-8) [9] is used due to the need of a high yield point of the metallic component and the galvanic corrosion compatibility between carbon and steel.
The selected CFRP is 8552/AS4 UD prepreg from Hexcel with 134 g/m², a widely used CFRP in the aerospace industry. The basic properties of these materials are given in Tab. 1.

Material	Tensile Stiffness E_1 (GPa)	Tensile Stiffness E_2 (GPa)	Density ϱ (g/cm³)
Steel 1.4310 [10]	178	178	7.9
CFRP 8552/AS4 [11]	141	10	1.58

Table 1: Material properties.

In order to assess the adhesion between the metal and CFRP two different lay-ups are used. The reference pure CFRP specimens consist of 16 layers UD $[0_{16}]$ whereas for the hybrid specimens the steel layer is positioned as the centre layer $[0_8/St/0_8]$. To increase comparability, the steel foil is chosen to 0.05 mm, as thin as possible during treatment. These lay-ups result in a laminate thickness of 1.98 mm for the reference beam and 2.03 mm for the hybrid beam.
Two plates per treatment method are manufactured and specimens are then cut by diamond sawing. Cure temperature is 180ºC as per prepreg manufacturer's recommendations.
Adhesion performance is evaluated by determination of the apparent inter-laminar shear strength by the short-beam method EN ISO 14130 [12] a three-point bending test. Specimen length is 20±0.1 mm and width is 10±0.1 mm.
Fig. 1 shows the dimensions of the hybrid specimen in which the difference to the reference beam specimen is that the steel layer is absent in the reference beam.

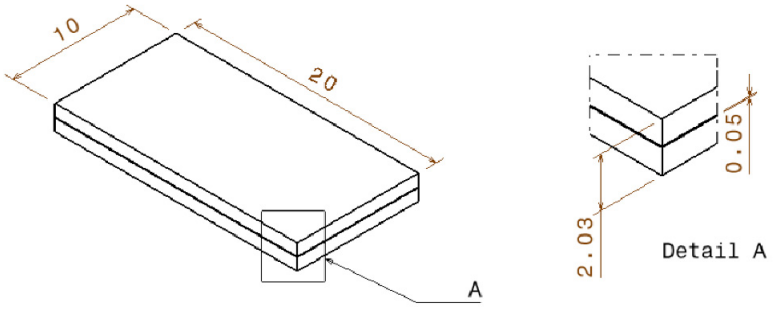

Figure 1: Dimensions of the short beam specimen.

The testing length, the distance between supports, is 9.9±0.1 mm with a radius of 2 mm. The radius of the loading member is 5mm. A testing machine Zwick 1476 with a maximum capacity of 100 kN was used. The displacement was measured with and LVDT placed in the movable part of the machine with a range of 49.5mm and accuracy below <0.1µm. Fig. 2 shows a schematic representation of the short beam fixture.

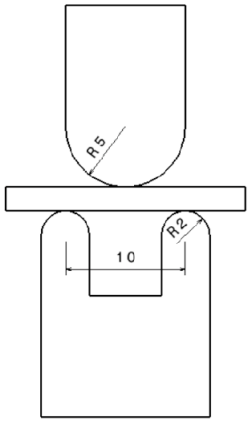

Figure 2: Schematic representation of the short beam fixture.

A standard surface treatment for stainless steel before adhesive joining is the 'Boeing sol-gel process'. Following this process, the material is degreased and then deoxidized by using a wet or dry grit-blasting method. Finally, an aqueous sol-gel system [13], a dilute solution of a stabilized alkoxy zirconium organometallic salt and an organosilane coupling agent, is applied. An adhesive coating is then applied to the treated surface to generate a durable bond [14]. This treatment is conducted in this work and regarded as a reference.
The surface treatment process can be subdivided into surface pre- and post-treatment. The pre-treatments are further differentiated into mechanical, physical, chemical and electrochemical treatments. The aim of the surface post-treatment process is to increase adhesion with the help of a coupling agent and to conserve the surface activity achieved by the pre-treatment. A surface treatment process always consists of a particular pre-treatment in combination with a particular post-treatment. As shown in Fig. 3, the sol-gel system is used in each approach, but an additional epoxy primer is applied only on the reference 'Boeing sol-gel'-specimens.

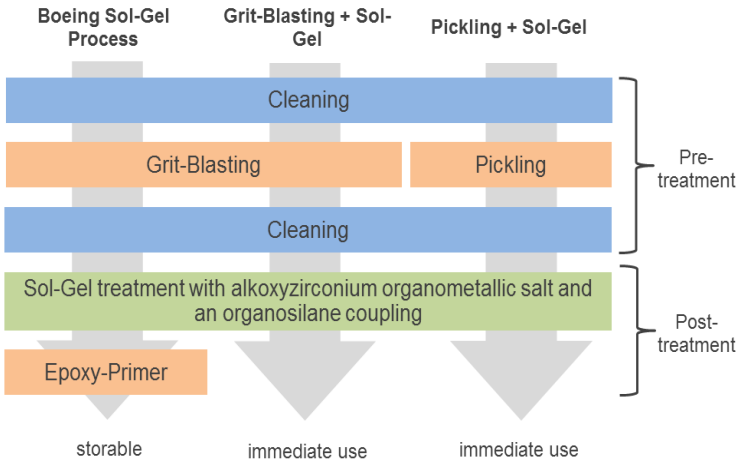

Figure 3: Schematic representation of the surface treatment process

Then different categories of pre-treatments for the steel foils are investigated. At first, grit-blasting is regarded and parameters as time, pressure, grit material and grit size are varied. After degreasing, the aqueous sol-gel is applied. As second category, vacuum blasting is examined, varying grit material as well as grit size. Finally, sol-gel is applied. As pickling is the most prevalent chemical pre-treatment for stainless steel [15], different pickling processes were examined to replace mechanical treatment of the thin steel foils. Specimens for the evaluation of the adhesion performance were fabricated using nitric-hydrofluoric and nitric-phosphoric-hydrofluoric acid as well as a nitrate-free solution consisting of hydrofluoric acid and hydrogen peroxide as oxidizing agent [16, 17]. Acid concentrations and pickling durations were varied and the pre-treated metal foils were rinsed with deionized water before drying in an oven. After drying, the foils were also post-treated with the aqueous sol-gel system.
Foils are laminated with prepreg within one hour after treatment to prevent environmental influences. However, as the manufacturing process may be constricted by this limitation, for one vacuum blasting configuration the foils were stored one day at room temperature with 50% relative humidity after treatment before positioning in the lay-up.
600 specimens were tested in total, whereas is was ensured by a second manufacturing and testing loop that 10 valid test results are existent for the most promising surface treatment configurations of each category, vacuum blasting, grit blasting, pickling and Boeing sol-gel process. Specimens manufactured utilizing these configurations and pure CFRP specimens were then additionally tested at different conditions. Dry specimens were tested at -55°C as well as 120°C and moisture saturated specimens were tested at room temperature.
Cure temperature is 180°C, therefore, comparing the hybrid specimens with pure CFRP-UD reference specimens it has to be considered that the curing shear stresses act on the same plane as the inter-laminar shear stresses. As curing temperature is above testing temperature, the differing coefficients of thermal expansion inevitably lead to residual stress in the laminate which can cause deformations. These inter-ply stresses may significantly lower the mechanical properties of the hybrid laminate, especially the residual inter-laminar shear strength. Different investigations have been performed to reduce residual stresses in pure composite as well as in fibre metal laminates, utilizing modified curing processes, an additional clamping tool to reduce thermal mismatch or post-stretching to reduce residual stress level of an already cured laminate [7]. However, these approaches are regarded in research only and the measurement of the residual stress level is

still unsatisfactory. Essentially, it has to be considered in the following investigations that these residual stresses increase with lower testing temperatures as the difference between manufacturing and testing temperature increases.

NUMERICAL MODELS

Numerical techniques in fracture modelling

There are two main techniques used to model fracture onset and fracture propagation: VCCT and CZM also known as cohesive elements, or in some literature as interface elements.

The VCCT technique is based on the principle that when a crack extends for a small amount the energy released in the crack propagation is equal to the work necessary to close the crack. This concept was first introduced by Rybicki and Kanninen [18] and developed further by Krueger [19]. In this technique the values of G_I, G_{II}, and G_{III} are computed from the nodal forces and displacements obtained from the solution of the finite element model. VCCT enables the calculation of these parameters in a single simulation. It does require however complex meshing techniques and an initial delamination. Therefore VCCT can predict crack propagation but not crack initiation.

Mendes [20, 21] examined the failure criteria for mixed mode delamination in glass/epoxy and CFRP/epoxy specimens. The purpose of an extensive program of tests was to determine the inter-laminar energy release rate of mode I, mode II, mixed-mode I+II, and mode III. The tests were DCB, ENF, MMB, and ECT.

Mendes calculated the energy release rate analytically, through the beam theory, and numerically through the VCCT technique. By comparing the experimental results with numerical simulations using VCCT Mendes concluded that the Power Law [22] criteria showed reasonable results in modes I+II, B-K [23] criteria had better results when Mode III was present. B-K extended to mode III as proposed by Reader [24] seems more convincing.

Cohesive elements are a more recent technique than VCCT. The concept of the cohesive elements is actual finite elements that are intended to model the resin layer between ply interfaces.

Cohesive elements are able to predict the onset and propagation of delamination without requiring pre-cracks. However, cohesive elements must be placed along all possible interfaces where delamination may occur.

In the proposed method [25, 26] a softening law for mixed-mode delamination can be applied to any interaction criterion. The constitutive equation of the cohesive elements uses a single variable, the maximum relative displacement, to track the damage at the interface under general loading conditions. The material properties required to define the element constitutive equation are:

i) the inter-laminar fracture toughness;

ii) the penalty stiffness,

iii) and the strengths.

The B–K interaction law requires additionally a material parameter η that is determined from standard delamination tests [25]. These elements have zero thickness and typically are rectangular elements with two nodes at each vertex as shown in Fig. 4.

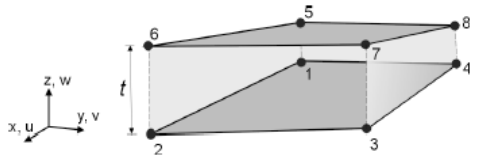

Figure 4: Zero thickness cohesive element. Figure retrieved from [25].

Ankersen and Davies [27] discuss some advantages and limitations of the cohesive elements by comparing two different constitutive laws of the cohesive elements: The bi-linear law and the exponential law. According to this research both constitutive laws are identical in delamination prediction. Exponential constitutive law is more appropriate to use with dynamic implicit solvers whereas the bi-linear constitutive law is more suited with explicit solvers. Mesh size is also a critical parameter in the cohesive elements technique due to the high stress gradients ahead of the cohesive zone. However for a sufficiently refined mesh the results are mesh independent.

The main characteristics of the two techniques are summarized in the Tab. 2.

In this research the numerical modelling is based on previous researches where cohesive elements were proposed and developed [25, 26, 28]. This is the main reason why the cohesive elements were used.

VCCT	Cohesive elements
• Requires nodal variables and topological information ahead and behind the crack front • Requires remeshing for crack propagation • Requires initial delamination • Predicts propagation of existing delamination	• Does not need an onset delamination • Predicts delamination initiation and propagation • Requires a refined mesh • Requires complex input parameters • Computationally expensive

Table 2: Summary of main features of VCCT and cohesive elements techniques

Finite element model

ABAQUS finite element code was used in all the numerical analysis in this work.
Two models were built. The reference beam with monolithic CFRP, and the hybrid beam with CFRP and the steel layer.
The main feature of these models is the use of zero thickness cohesive elements.
The geometrical model took advantage of the symmetries in the three-point bending test. Only one half of the beam's length was modelled applying a proper boundary condition in the mid span. The model has a unit width with appropriate symmetry boundary conditions on both faces parallel to the lengthwise direction of the beam (x-direction). The negligible Poisson effect in the y-direction allows this simplification. Fig. 5 shows the actual beam of 20mm x 10mm (represented in transparency) and the finite element geometric model 5mm x 1mm.

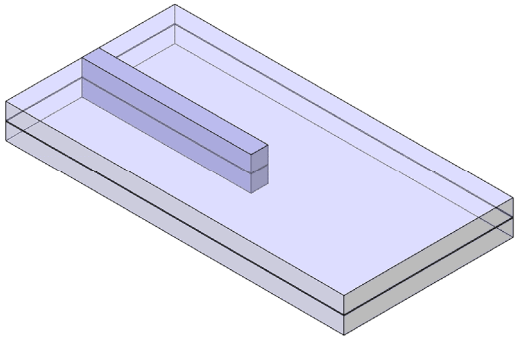

Figure 5: Short beam (in translucent grey) and geometrical model of the beam (in solid grey) for finite element simulation.

The reference beam was modelled with one layer of zero thickness cohesive elements in the neutral fibre and the hybrid beam was modelled with zero thickness cohesive elements in the interface between the CFRP and the steel.
The models have 8 elements per thickness in the CFRP and 40 elements across length with a bias ratio of 4, i.e. 40th element in mid-span is 4 times smaller than the 1st element in the extreme of the beam. The largest element has 0.460mm in length and the smaller element has 0.115 mm in length.
The FEM model of the reference beam has:

- 640 cubic 8 node C3D8R elements with reduced integration: 320 elements for each half thickness.
- 40 COH3D8 zero thickness cohesive elements in the neutral fibre.
- 1478 nodes.
- 5400 DOF's.

The FEM model of the hybrid beam has:

- 680 cubic 8 node C3D8R elements with reduced integration: 320 elements for each half thickness plus 40 elements in the steel layer.
- 80 COH3D8 zero thickness cohesive elements: 40 elements on each CFRP/Steel interface
- 1640 nodes.
- 5892 DOF's.

Fig. 6 shows the FEM model of the hybrid beam in ABAQUS:

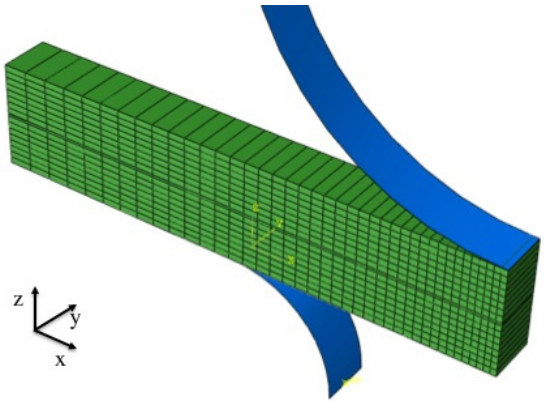

Figure 6: Model of the unit width hybrid beam Loading member and support modelled as rigid bodies.

The cohesive elements use the Quadratic Nominal Stress Criterion (QUADS) shown in Eq. 1.

$$\left\{\frac{\langle t_n \rangle}{t_n^0}\right\}^2 + \left\{\frac{t_s}{t_s^0}\right\}^2 + \left\{\frac{t_t}{t_s^0}\right\}^2 = 1 \tag{1}$$

The variables t_n, t_s, t_t are the normal stress and the shear tensions on both directions respectively of the cohesive models. The variables t_n^0, t_s^0, t_t^0 are the damage threshold values of the cohesive elements. The Macaulay operator in the normal stress $\langle t_n \rangle$ is used to ensure that the damage does not occur when $t_n < 0$.

The damage evolution of the cohesive elements uses the mixed mode criterion proposed by Benzeggagh and Kenane, the B-K criterion [23]. This criterion accounts for the variation of fracture toughness as function of the mode ratio.

In order to match the experimental result with the numerical simulation several values of G_{IIC} were tested as the dominant failure mode in this test is Mode II (Tab. 3).

In order to replicate the actual test, the numerical model has to include the contact interaction between the beam and the loading member and the beam and the support.

A penalty formulation was established for the contact properties and interaction definition was set to surface to surface interaction.

Simulations with contact formulation are prone to severe discontinuous nonlinearities. Therefore the entire displacement was divided by 10 equal steps of 0.1mm to reduce severe discontinuities in the solver.

The accumulated effect of cohesive elements with damage model and damage evolution, and the contact formulation causes a very intense computational effort. Some initial settings of the steps module, namely the tolerances of the Line Search control parameters and the Time Incrementation parameters had to be increased from their initial settings in order to enable the solver to reach a solution.

RESULTS AND ANALYSIS

Experimental results

The apparent inter-laminar shear strength for the reference beam (monolithic CFRP) was calculated based on the load measured by the testing machine using Eq. (2) [12]:

$$\tau = \frac{3}{4} \cdot \frac{F}{b \cdot h} \tag{2}$$

where:

F is the load in (N),

b and h are the width and thickness of the specimens respectively (mm),

τ is the apparent inter-laminar shear strength (MPa).

For hybrid beams however a modified version of Eq. (2) is used to account for the different stiffness of the constituents in the laminate [3]:

$$\tau = \frac{3}{4}\cdot\frac{F}{b}\cdot\frac{s^2 - t^2}{(s-t)^3 - 3\cdot(s-t)\cdot(s+t)^2 + 4t^3\cdot\frac{E_{metal}}{E_{CFRP}}} \tag{3}$$

where:

s and t are the specimen thickness and metal layer thickness in millimetres respectively

E_{metal} and E_{CFRP} are the elastic modulus of the metal and CFRP respectively in GPa.

Eq. (1) and (2) were used for every individual width and thickness of the specimens as they differ slightly from nominal dimensions due to manufacturing tolerances. Tab. 3 presents the experimental results with the average maximum ILSS for all types of beams and a comparison between the reference beam and the hybrid beams. The average maximum ILSS is in the range of [125 MPa – 130 MPa] which corresponds to a maximum load of [3.4kN – 3.5 kN]

Types of beams	$\overline{ILSS}$ (MPa)	$std\left(\overline{ILSS}\right)$ (MPa)	$\overline{ILSS}_{Hybrid} - \overline{ILSS}_{Reference}$ (MPa)	$\overline{ILSS}_{Hybrid} / \overline{ILSS}_{Reference}$
Reference beam	130.03	1.40	-	-
Vacuum Blasting (one day storage)	129.87	3.76	-0.16	0.999
Vacuum Blasting	128.20	2.36	-1.83	0.986
Grit Blasting	126.11	5.00	-3.92	0.970
Pickling	125.63	2.15	-4.4	0.966

Table 3: ILSS Experimental results – Comparison between reference beam and the hybrid beams with different surface treatments.

Fig. 7 shows the typical behaviour of reference and hybrid specimens: An almost linear elastic displacement, followed by a gradual yielding of the resin rich neutral fibre (in the case of the reference beam) or CFRP/metal interface (in the case of the hybrid beam), until the beam reaches its maximum load. Failure occurs shortly after. The crack propagates in one of two ways: By a sudden and continuous propagation or by several steps due the heterogeneity of the resin.

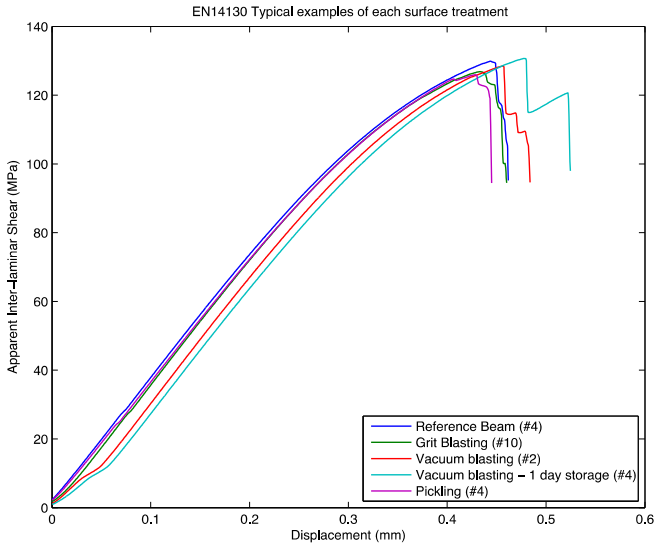

Figure 7: Plot of typical examples of Reference beam and Hybrid beam with vacuum blasting.

Numerical Results

From the finite element model the displacement and the reaction force of the loading member were extracted. From these two data sets the apparent inter-laminar shear stress was calculated using Eq. (2) and (3) for the reference beam and the hybrid beam respectively.

Tab. 4 presents the numerical results and compares them with the experimental results. In the upper part of the table is the average experimental ILSS and the numerical ILSS for several values of G_{IIC} of the reference beam. Similarly in the lower part of the table is the average ILSS and the numerical ILSS for several values of G_{IIC} of the vacuum blasting tests.

Reference Beam	ILSS (MPa)	Difference
Experimental	$\overline{130.03}$	-
Numerical		
G_{IIC} =1.1 N.mm^{-1}	132.90	2.2%
G_{IIC} =1.0 N. mm^{-1}	123.70	4.9%
G_{IIC} =0.8 N. mm^{-1}	110.10	15.3%
G_{IIC} =0.9 N. mm^{-1}	101.40	22.0%
Hybrid Beam	**ILSS (MPa)**	**Difference**
Experimental	$\overline{128.20}$	-
Numerical		
G_{IIC} =1.0 N.mm^{-1}	123.68	3.5%
G_{IIC} =1.1 N.mm^{-1}	132.94	3.7%
G_{IIC} =0.9 N.mm^{-1}	113.49	11.5%
G_{IIC} =0.8 N.mm^{-1}	110.14	14.1%

Table 4: Comparison between experimental average results and numerical results

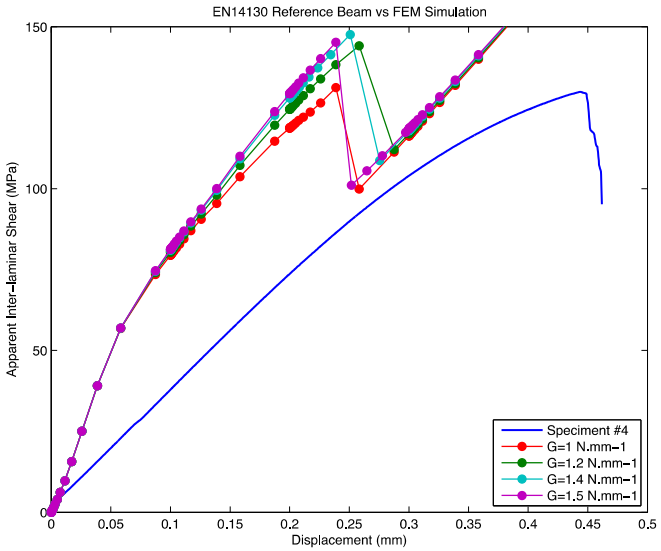

Figure 8: Reference beam. Comparison between numerical and experimental results (specimen #4).

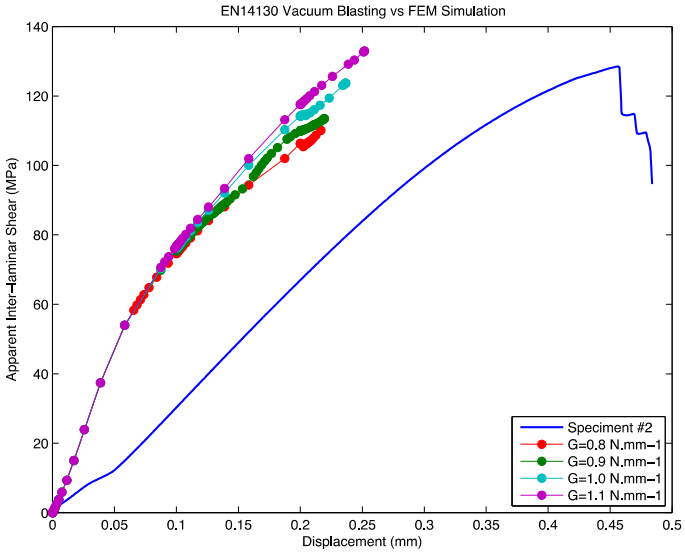

Figure 9: Hybrid beam. Comparison between numerical and experimental results (specimen #2).

Fig. 8 and Fig. 9 show the plots of several numerical simulations for several values of G_{IIC} for the reference beam and the hybrid beam respectively. Fig. 8 shows an initial linear trend followed by a slight decrease in slope. This decrease is the beginning of the yielding of the cohesive elements. The load increases at an apparently linear rate until it reaches its peak. After the peak there is a sudden drop in the apparent shear stress load indicating the unstable crack propagation. After the shear stress increases again. This increase is the result of the reaction of two half beams fully delaminated one above the other and it is no longer meaningful. In the case of the reference beam the solver is able to converge to a solution in every step.
In the case of the hybrid beam after the peak shear stress the ABAQUS solver is unable to converge to a solution of its current step. This is due to the fact that in the case of an unstable crack propagation the kinetic energy associated with it is relevant and it's not considered in an ABAQUS implicit analysis. However the maximum load is correctly calculated by the solver.
One common feature of either the reference or hybrid beams is that the stiffness of the numerical simulation is higher than the stiffness of the experimental results. This discrepancy is analysed in the next section.

DISCUSSION

The numerical models predict a maximum ILSS shear strength close to the experimental maximum ILSS provided that the proper G_{IIC} is set. The results predicted by the numerical models have a higher stiffness than the stiffness of the experimental tests.
There are several factors that contribute for this discrepancy:

i. In the experimental tests the displacement is measured by an LVDT above the specimen in the movable part of the testing machine while in the numerical simulation the displacement is measured directly in the loading member. The effect of the compliance of the testing machine is therefore expected;
ii. There is an unavoidable initial slack in the experimental test that does not occur in the numerical simulation;
iii. The testing machine has some elasticity that, however small, cannot be ignored.

The first factor is considered as the most relevant. In these tests the measured displacement until failure is extremely low (≈ 0.45mm). It is possible that the LVDT may be unable to measure accurately the displacement in such a small range.
There is also a small contribution of the initial slack of the testing fixtures. It is observed some irregular data in the beginning of the experimental tests plots.
The third factor is the less significant. The maximum measured loads [3.4 kN – 3.5 kN] are far lower than the maximum capacity of the testing machine (100 kN).
These accumulated factors, although in different weights, are responsible for the discrepancy in slope between the numerical and experimental curves.
The experimental results show that the maximum ILSS of the hybrid beams is very close to the ILSS of the reference beam. Vacuum blasting surface treatment is clearly the best in terms of hybrid ILSS performance. The one day storage between surface treatment and composite manufacturing does not affect ILSS performance. The remainder surface treatments are clearly less competitive.
The numerical results show that with a proper adjustment of the critical energy release rate G_{IIC} it is possible to predict accurately the maximum load (therefore the ILSS) of both the reference and hybrid beams.
The standard deviation of the ILSS of the hybrid beams is considerably higher that the reference beam. It is also noted that the standard deviation of the treatment with one day storage is higher than the same treatment with no storage. However, it is unlikely that it will have an impact in actual aircraft design due to the conservative factor of safety of composite aircraft structures.
The short beam test method was chosen due to the previous experiences in assessing ILSS in hybrid composites [2],[6].
The small size of the specimens does not affect a purely experimental research where different specimens are compared and any eventual effect of the compliance of the testing machine has an identical impact in all results.
However, it poses a greater difficulty when trying to replicate the test in a FEM simulation because the eventual effect of the compliance of the testing machine is increased with specimens that have such a small displacement. It is suggested therefore that in a future research of inter-laminar shear stress by three-point bending the size of the specimens should be bigger than the size prescribed by EN14130 in order to reduce the effect of the factors that induce uncertainty in this test.

CONCLUSIONS AND FUTURE WORK

Hybrid CFRP/Steel composites have a maximum ILSS very close to the ILSS of a reference beam.
Hybrid CFRP/Steel composites are a competitive and cost effective alternative to CFRP/Ti alloy. It has a similar maximum ILSS while the cost of the austenitic steel is significantly lower than the cost of Ti alloys.
Vacuum blasting is the surface treatment that withstands higher ILSS from all the tested surface treatments. It is also simpler than pickling or grit blasting.
The vacuum blasting treatment with one day storage has a maximum apparent ILSS close to the reference beam (less 0.16 MPa). This shows that the one day storage between treatment and lay-up does not affect the shear stress capability. This is a very important advantage in terms of manufacturing process.
The FEM model is able to predict the maximum ILSS of the hybrid CFRP/Steel beam which is the main engineering parameter.
The discrepancy between the measured displacement and the numerical displacement is not fully understood. Although the available data suggests that it is due to the compliance of the testing machine, only a dedicated test program to determine the eventual compliance using DIC technology [29] would definitely demonstrate the effect of the compliance
The size of the specimens prescribed by EN14130 is very small. This small size enhances the effect of the compliance of the testing machines. It is suggested therefore that in a future research of inter-laminar shear stress by three-point bending the size of the specimens should be bigger than the size prescribed by EN14130 in order to reduce the effect of the factors that induce uncertainty in this test.
The short beam tests have some shortcomings, particularly when comparing with numerical simulations. It involves contact formulation and the shear stress is an induced stress caused by transverse shear of the loading member. These disadvantages leads to a next step of the study of shear stress of hybrid CFRP/Steel composites that is the single lap shear tests (SLS).

ACKNOWLEDGEMENTS

The first author's research is supported by the research grant BD/51597/2010 provided by the Portuguese Foundation for Science and Technology.
The support of the Institute of Composite Structures and Adaptive Systems of the German Aerospace Centre in the manufacturing and testing of the specimens is acknowledged.

ACRONYMS AND DEFINITIONS

CFRP – Carbon Fibre Reinforced Polymer
CTE – Coefficient of Thermal Expansion
CZM – Cohesive Zone Method
DCB – Double Cantilever Beam
DIC – Digital Image Correlation
ECT – Edge Crack Torsion
ENF – End Notch Flexure
FEM – Finite Element Method
ILSS – Inter-laminar Shear Stress
LVDT – Linear Variable Differential Transformer
MMB – Mixed Mode Bending
QUADS – Quadratic Nominal Stress Criterion
SLS – Single Lap Shear
VCCT – Virtual Crack Closure Technique

REFERENCES

[1] ESD Symposium Committe, ESD Terms and Definitions (Version 12), Massachussets Institute of Technology Engineering Systems Division, (2001).

[2] Fink, A., Kolesnikov, B., Hybrid titanium composite material improving composite structure coupling, In: Spacecraft Structures, Materials and Mechanical Testing 2005, 581 (2005) 135.
[3] Kolesnikov, B., Herbeck, L., Fink, A., CFRP/titanium hybrid material for improving composite bolted joints, Compos. Struct., 83(4) (2008) 368–380.
[4] Camanho, P.P., Fink, A., Obst, A., Pimenta, S.,Hybrid titanium–CFRP laminates for high-performance bolted joints, Compos. Part Appl. Sci. Manuf., 40(12) (2009) 1826–1837.
[5] Fink, A., Camanho, P. P., Andrés, J. M., Pfeiffer, E., Obst, A., Hybrid CFRP/titanium bolted joints: Performance assessment and application to a spacecraft payload adaptor, Compos. Sci. Technol., 70(2) (2010) 305–317.
[6] Fink, A., Camanho, P., Reinforcement of composite bolted Joints by means of local metal hybridization,Composite joints and connections, Pedro Camanho and Liyong Tong, Eds. Woodhead Publ., (2011).
[7] Stefaniak, D., Kappel, E., Kolotylo, M., Huhne, C., Experimental identification of sources and mechanisms inducing residual stresses in multi layered fiber-metal laminates, In: Euro-Hybrid 2014, PFH – Private University of Applied Sciences, Stade, Germany, (2014).
[8] Kim, H. S., Park, S. W., Hwang, H. Y., Lee, D. G., Effect of the smart cure cycle on the performance of the co-cured aluminum/composite hybrid shaft, In: Thirteen. Int. Conf. Compos. Struct. Iccs13, 75(1–4) (2006) 276–288.
[9] Lamineries Matthey SA. Stahl 1.4310.
[10] De Freitas, M., Reis, L., Li, B., Comparative study on biaxial low-cycle fatigue behaviour of three structural steels, Fatigue Fract. Eng. Mater. Struct., 29(12) (2006) 992–999.
[11] Marlett, K., Hexcel 8552 IM7 Unidirectional Prepreg 190 gsm & 35%RC Qualification Material Property Data Report, FAA, FAA Special Project Number SP4614WI-Q, (2011).
[12] EN 14130 Fibre-reinforced plastic composites Determination of apparent interlaminar shear strength by short-beam method, (1998).
[13] Mazza, J.J., Sol-Gel Technology for Low-VOC, Nonchromated Adhesive Bonding Applications SERDP; Project PP-1113, Task 1. Storming Media, (2004).
[14] Rider, A., Williams, I., Shum, E., Mirabella, L., Environmental durability trial of bonded composite repairs to metallic aircraft structure, DTIC Document, (2005).
[15] Covino, B. S., Scalera, J. V., Fabis, P. M., U. S. B. of Mines, Pickling of stainless steels–a review. United States Dept. of the Interior, Bureau of Mines, (1984).
[16] Stefaniak, D., Kappel, E., Kolesnikov, B., Hühne, C., Improving the mechanical performance of unidirectional CFRP by metal-hybridization, In: ECCM15 - 15th European Conference on Composite Materials, Venice, Italy, (2012).
[17] Narváez, L., Cano, E., Bastidas, J. M., Effect of ferric ions in AISI 316L stainless steel pickling using an environmentally-friendly H_2SO_4-HF-H_2O_2 mixture, Mater. Corros., 54(2) (2003) 84–87.
[18] Rybicki, E. F., Kanninen, M. F., A finite element calculation of stress intensity factors by a modified crack closure integral, Eng. Fract. Mech., 9(4) (1977) 931–938.
[19] Krueger, R., The Virtual Crack Closure Technique: History, Approach and Applications, NASA, NASA/CR-2002-211628 ICASE Report No. 2002-10, (2002).
[20] Marat-Mendes, R., Critérios de delaminação em materiais compósitos sob solicitações multiaxiais, PhD Thesis in Mechanical Engineering, Universidade Técnica de Lisboa - Instituto Superior Técnico, Lisboa, (2009).
[21] Marat-Mendes, R. M., Freitas, M. M., Failure criteria for mixed mode delamination in glass fibre epoxy composites, Compos. Struct., 92(9) (2010) 2292–2298.
[22] Whitcomb, J. D., Analysis of instability-related growth of a through-width delamination, National Aeronautics and Space Administration, Langley Research Center, Technical Report NASA-TM-86301, NAS 1.15:86301, (1984).
[23] Benzeggagh, M. L., Kenane, M., Measurement of mixed-mode delamination fracture toughness of unidirectional glass/epoxy composites with mixed-mode bending apparatus, Compos. Sci. Technol., 56(4) (1996) 439–449.
[24] Reeder, J. R., 3D mixed-mode delamination fracture criteria–an experimentalist's perspective, In: American Society for Composites 21st Annual Technical Conference, Dearborn, MI; United States, (2006).
[25] Camanho, P. P., Dávila, C. G., Mixed-mode decohesion finite elements for the simulation of delamination in composite materials, Nasa-Tech. Pap., 211737(1) (2002) 33.
[26] Camanho, P. P., Davila, C. G., De Moura, M. F., Numerical simulation of mixed-mode progressive delamination in composite materials, J. Compos. Mater., 37(16) (2003) 1415–1438.
[27] Ankersen, J., Davies, G. A. O., Interface elements-advantages and limitations in CFRP delamination modelling, In: 17th International Conference on Composite Materials, Edinburgh, UK, (2009).
[28] Turon, A., Davila, C. G., Camanho, P. P., Costa, J., An Engineering Solution for Solving Mesh Size Effects in the Simulation of Delamination with Cohesive Zone Models, (2007).

[29] Pan, B., Qian, K., Xie, H., Asundi, A., Two-dimensional digital image correlation for in-plane displacement and strain measurement: a review, Meas. Sci. Technol., 20(6) (2009) 062001.